

Occurrence and stability of ferromagnetism in chemically synthesized cobalt doped TiO₂

K. M. Reddy · A. Punnoose

Received: 6 January 2007 / Accepted: 29 January 2007
© Springer Science+Business Media, LLC 2007

Abstract We report the development of ferromagnetism in ~30 nm sized well-characterized Ti_{1-x}Co_xO₂ powders with $x = 0.00015\text{--}0.006$ and its absence for $x > 0.006$. In addition, these studies show the effect of Co doping on the structural stability and anatase to rutile phase transformation. X-ray diffraction data of samples synthesized by a wet chemical method and annealed at 450 °C indicate a limited solubility of ~1.2% for Co in the anatase TiO₂ matrix, and with further increase, the CoTiO₃ phase is formed along with increased presence of rutile TiO₂. The bandgap (~3.23 eV) of the anatase TiO₂ remained almost unchanged for $x < 0.006$, but decreased rapidly for $x \geq 0.006$ approaching 2.8 eV for $x = 0.03$. The magnetic data from Ti_{1-x}Co_xO₂ samples with $x = 0.006$ showed a coercivity $H_c \sim 150$ Oe and a weak magnetic moment of 0.2 μ_B /ion at 300 K. The ferromagnetism of Ti_{0.994}Co_{0.006}O₂ with open hysteresis loops continue up to a high superparamagnetic blocking temperature $T_B \sim 675$ K, above which a superparamagnetic behavior was observed. Systematic changes in the structural, magnetic and optical properties suggest that Co doping is an excellent method to tailor the physical properties of TiO₂ nanoparticles.

1 Introduction

The discovery of room-temperature ferromagnetism (FM) by Matsumoto et al. [1] in transition metal doped anatase TiO₂ thin films encouraged a tremendous

experimental and theoretical research effort focused on understanding the FM of this doped metal oxide. Since then, various research groups [2–11] have investigated the above room-temperature FM experimentally and theoretically in anatase and rutile Ti_{1-x}Co_xO₂ systems prepared under different synthesis conditions and attributed the FM to different mechanisms/origins that are based on oxygen deficiencies, Co metal impurity segregation and/or electron/hole mediated mechanisms. Shinde et al. [2] found 20–50 nm cobalt cluster formation in PLD films with a smaller fraction of Co ions incorporating into the TiO₂ matrix and observed ferromagnetism at higher temperatures. Park et al. [6] reported ferromagnetism due to Co ions in rutile TiO₂ films. Ferromagnetism induced by a small amount of Co clusters is also observed using magnetic circular dichroism studies on anatase Ti_{1-x}Co_xO₂ films [8]. Griffin et al. [9] have reported ferromagnetism in insulating anatase films, suggesting that free carriers do not necessarily contribute to the ferromagnetism. Chemically synthesized colloidal nanocrystals of Co doped TiO₂ showed a stronger ferromagnetic behavior and do not indicate any sort of impurity formation [3], signifying alternative routes to prepare DMS materials. The materials prepared using deposition techniques in reducing atmospheres could often produce segregation of magnetic dopants especially when used at concentration exceeding the solubility limits. It is therefore vital to prepare these materials using wet chemical routes in oxidative environments, which will intrinsically eliminate the formation of metallic clusters and confirm intrinsic FM. In this paper, we describe the room-temperature FM resulting from Ti_{1-x}Co_xO₂ nanoparticles prepared by a sol–gel mediated hydrolysis method with a very wide range of Co concentration

K. M. Reddy · A. Punnoose (✉)
Department of Physics, Boise State University, Boise,
ID 83725-1570, USA
e-mail: apunnoos@boisestate.edu

x , varying from $0.00015 < x < 0.1$. Interestingly, $\text{Ti}_{1-x}\text{Co}_x\text{O}_2$ nanoparticles with low Co contents showed FM with saturation magnetization, remanance and coercivity varying systematically. Further, the effect of Co doping on structural stability of TiO_2 nanoparticles and anatase–rutile phase transformation is also discussed.

2 Experimental

Appropriate amounts of titanium isopropoxide, isopropyl alcohol and acetic acid were added to deionized water to obtain a clear solution. To this solution a required amount of 0.5 M CoCl_2 was added and stirred vigorously. NH_4OH (~30.0% NH_3) was added as the hydrolyzing agent until the pH of the solution was 9. The resulting precipitate was washed to remove any chloride by-products and annealed in air for 3 h at 450 °C. X-ray diffraction (XRD) spectra were recorded at room temperature on a Phillips X'Pert X-ray diffractometer with a CuK_α source ($\lambda = 1.5418 \text{ \AA}$) in Bragg-Brentano geometry. High-resolution transmission electron microscopy (TEM) analysis was carried out on a JEOL JEM 2010 microscope operating at 200 kV and image processing was carried out using the Digital Micrograph software from Gatan (Pleasant, California, USA). Energy dispersive X-ray spectroscopy (EDS) was carried out using the Oxford Link system attached on the TEM. Room-temperature optical spectra in the ultraviolet and visible light wavelength ranges were collected using a CARY 5000 spectrophotometer fitted with an integrating sphere diffuse reflectance accessory. Magnetic measurements were carried out as a function of temperature (4–350 K) and magnetic field (0 to ± 65 kOe) using a commercial magnetometer (Quantum Design, PPMS) equipped with a superconducting magnet. The data reported here were corrected for the background signal from the sample holder (clear plastic drinking straw) with diamagnetic susceptibility $\chi = -4.1 \times 10^{-8} \text{ emu/Oe}$. Data analyses were carried out using Mathsoft's Mathcad. High temperature magnetic measurements were carried out using a LakeShore vibrating sample magnetometer equipped with a high temperature (300–1,000 K) oven.

3 Results and discussion

XRD patterns of powder $\text{Ti}_{1-x}\text{Co}_x\text{O}_2$ samples annealed at 450 °C showed (Fig. 1a) strong peaks of tetragonal anatase and rutile phase. For comparison, JCPDS data from anatase, rutile and CoTiO_3 phases

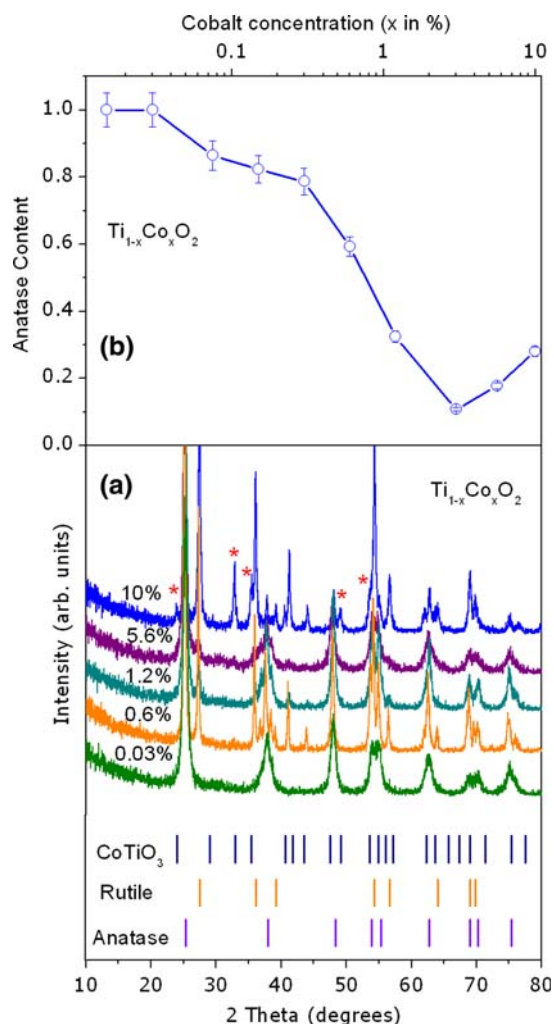


Fig. 1 (a) Powder X-ray diffraction patterns recorded on $\text{Ti}_{1-x}\text{Co}_x\text{O}_2$ samples prepared by annealing the reaction precipitate at 450 °C. Reference patterns of anatase, rutile and CoTiO_3 are given for comparison. * indicates peaks arising from CoTiO_3 phase. (b) The variation of anatase phase TiO_2 in the $\text{Ti}_{1-x}\text{Co}_x\text{O}_2$ samples with increasing Co concentration

are also given. The phase composition of the samples was obtained from the following equation [12], $x_A = 1/[1 + 1.26(I_R/I_A)]$, where x_A is the weight fraction of anatase in the mixture, and I_A and I_R are the peak intensities of the anatase (101) and rutile (110) diffractions, respectively. For $x \leq 0.03$, the samples showed pure anatase TiO_2 phase and above this doping range, the rutile phase started appearing and its relative concentrations increased linearly with cobalt concentration. The ionic size of tetrahedral Ti^{4+} in anatase (0.42 Å) is much smaller than the Co^{2+} and Co^{3+} ions and therefore Co incorporation into the TiO_2 host lattice is likely to produce significant changes in the structural properties due to the difference in the ionic size and charge [13]. No trace

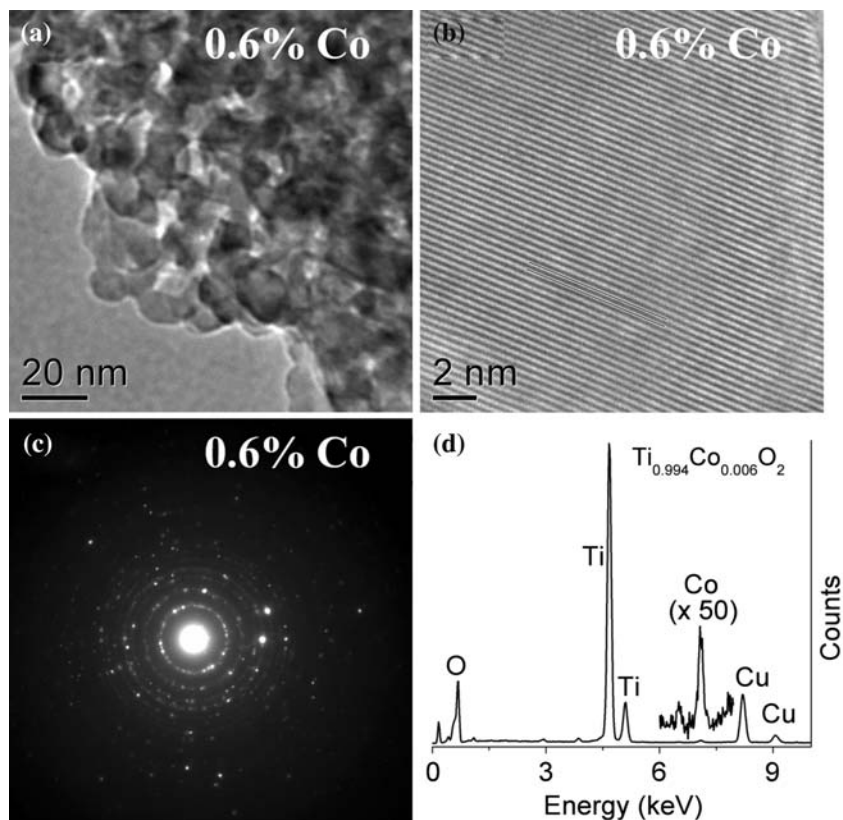
of cobalt metal, oxides or any binary titanium–cobalt phases were observed in any of the samples doped up to 1.2%. However, for $x > 1.2\%$, a mixed CoTiO_3 impurity phase started appearing as confirmed by XRD. It is interesting to note that the anatase phase was decreasing with increasing cobalt concentration (Fig. 1b) although the anatase phase is very stable up to 700 °C in undoped TiO_2 . Average crystallite size L of the anatase $\text{Ti}_{1-x}\text{Co}_x\text{O}_2$ phase was calculated using the width of the (101) peak, and the Scherrer relation, $L = 0.9\lambda/B \cos \theta$ (where θ is the peak position, λ is the X-ray wavelength and $B = (B_m^2 - B_s^2)^{1/2}$ was estimated using the measured peak width B_m and the instrumental width B_s) and the estimated crystallite sizes varied in the 10–40 nm range.

High-resolution TEM images from the 0.6% Co doped TiO_2 sample showed (Fig. 2a and b) an average particle size of ~25 nm, comparable to the estimates from XRD. Electron diffraction patterns of 0.6% Co doped sample (Fig. 2c) taken from an aggregate of particles revealed the characteristic ring patterns of TiO_2 that confirms the structure and phase measured by XRD. Energy dispersive X-ray analysis (shown in Fig. 2d) confirmed the increasing level of Co doping in the $\text{Ti}_{1-x}\text{Co}_x\text{O}_2$ samples with increasing x .

The optical properties of the samples were characterized by measuring the diffuse reflection percentage in 300–600 nm wavelength range. Figure 3a shows the reflectance (in %) versus wavelength plot for $\text{Ti}_{1-x}\text{Co}_x\text{O}_2$ powders which have absorption edges in 375–400 nm range. The diffuse reflectance, R is related to the Kubelka-Munk function $F(R)$ by the relation, $F(R) = (1 - R)^2/2R$, where R is the percentage reflectance [14]. The band gap energies of the $\text{Ti}_{1-x}\text{Co}_x\text{O}_2$ powders were calculated from their diffuse-reflectance spectra by plotting the $F(R)^2$ versus E (eV). The linear part of the curve was extrapolated to $F(R)^2 = 0$ to get the direct band gap energy. The band gap energy for $\text{Ti}_{1-x}\text{Co}_x\text{O}_2$ decreased with cobalt doping and is shown in Fig. 3b. From these calculations the direct bandgap energy for pure anatase and rutile phases was found to be 3.23 and 3.01 eV, respectively, which is consistent with the existing reports. A decrease in bandgap energy due to TM doping has been observed in other systems also [15].

Magnetic measurements carried out on pure TiO_2 nanoparticles showed the expected diamagnetism with a negative magnetic susceptibility. Magnetization M versus applied magnetic field H data from few selected samples is shown in Fig. 4a. Up to a Co doping concentration of 0.6%, the $\text{Ti}_{1-x}\text{Co}_x\text{O}_2$ samples are

Fig. 2 TEM data of 0.6% Co doped TiO_2 nanoparticles showing (a) the average particle size, (b) high resolution image depicting good crystallinity and the lattice spacings, (c) electron diffraction pattern and (d) energy dispersive X-ray data



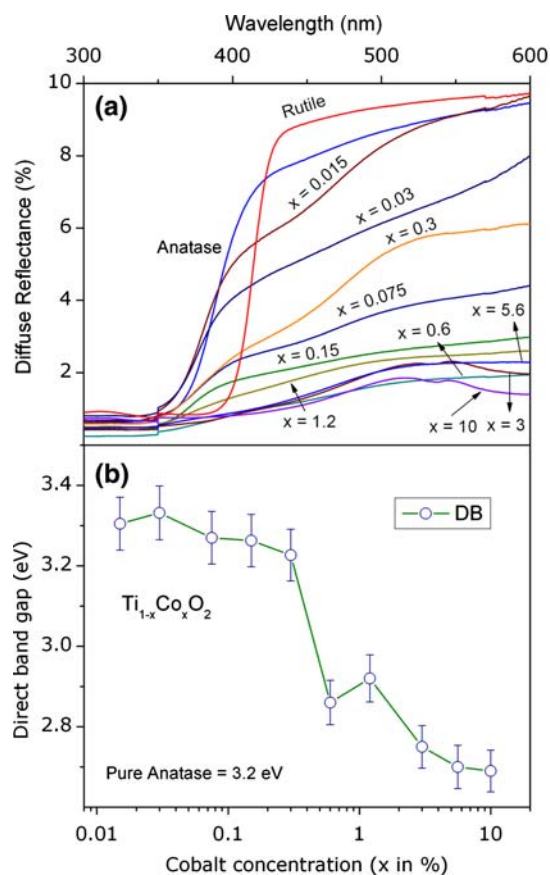


Fig. 3 (a) UV–VIS spectra recorded in % reflection mode for different Co doped TiO_2 . (b) Direct band gap energy values estimated from the data in panel (a) as a function of Co concentration

ferromagnetic at room temperature. The samples with $\geq 1.2\%$ Co merely showed a linear M versus H variation at 300 K indicative of pure paramagnetic behavior (see top inset of Fig. 4a). Figure 4a presents the room-temperature hysteresis loop for $\text{Ti}_{0.994}\text{Co}_{0.006}\text{O}_2$ nanoparticles showing coercivity $H_c \sim 150$ Oe (Fig. 4a bottom-inset) and a magnetic moment of $0.2 \mu_B/\text{Co}$. Although the magnetic moment obtained in our samples are comparable to that reported in some recent studies [2, 16, 17], much higher moments have been reported from samples prepared using deposition techniques [5, 18]. Figure 4b shows the variation of the room-temperature remanence M_r and saturation magnetization M_s of 450°C prepared $\text{Ti}_{1-x}\text{Co}_x\text{O}_2$ as a function of Co concentration. Also, the coercivities of the samples varied in the 15–150 Oe range. The ferromagnetic behavior constantly improves with x up to 0.6% Co doping, however, the FM was destroyed completely and only a pure paramagnetic phase was observed for $x > 0.006$. This is qualitatively similar to that observed by the authors in Co doped SnO_2

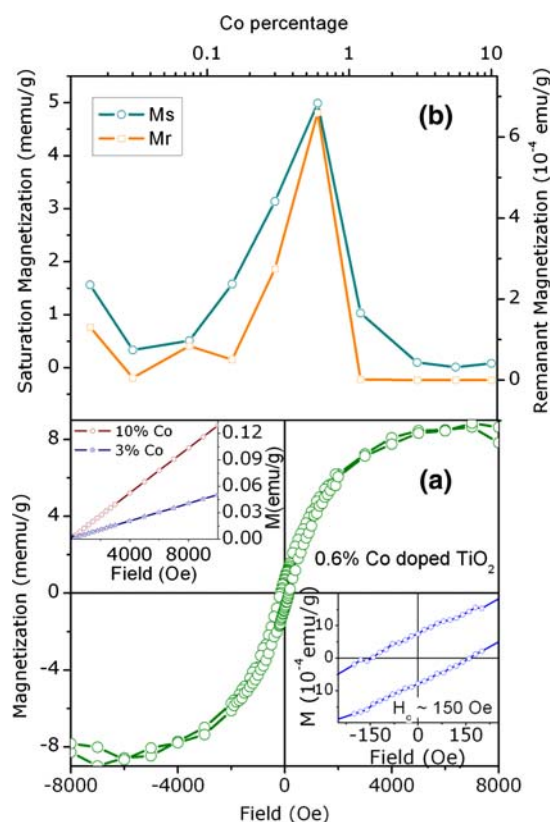
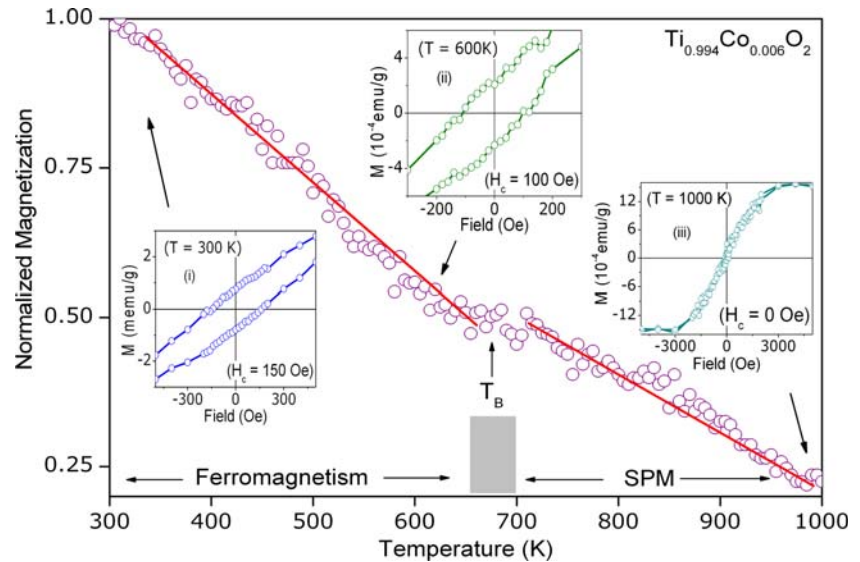


Fig. 4 (a) Room temperature hysteresis loop measured on 0.6% Co doped TiO_2 , bottom inset shows the low field region, illustrating the coercive field. Top inset (top) shows the M – H plots of the paramagnetic samples with $x > 0.006$. (b) Shows variation of saturation magnetization M_s and remanent magnetization M_r of the $\text{Ti}_{1-x}\text{Co}_x\text{O}_2$ samples with the different Co%

nanoparticles in which the ferromagnetism was destroyed when $x > 0.01$ [19]. The anatase phase of $\text{Ti}_{1-x}\text{Co}_x\text{O}_2$ is present in all samples for $x \leq 0.1$, although its fraction is much less in samples with $>1\%$ Co, increased presence of rutile TiO_2 phase and the mixed phase CoTiO_3 might be one possible reason for the absence of ferromagnetism when $x > 0.006$. Complete absence of ferromagnetism in samples with $x > 0.001$ rules out the possibility of any impurity phase being the origin of ferromagnetism. Coey et al. [20, 21] has shown that ferromagnetism is more prominent in TM doped oxide semiconductors when the dopant concentration is lower. Increasing the concentration to above the percolation limit changes the magnetic interaction antiferromagnetic and will destroy ferromagnetism. In Co doped SnO_2 , Hays et al. [19] have shown that Co enters into interstitial sites for $x > 0.01$ leading to significant structural disorder and destruction of ferromagnetism. The systematic changes in the anatase to rutile phase change and the magnetic behavior with increasing x in $\text{Ti}_{1-x}\text{Co}_x\text{O}_2$ nanoparticles

Fig. 5 M versus T variation of $\text{Ti}_{0.994}\text{Co}_{0.006}\text{O}_2$ sample measured with an applied magnetic field of 8,000 Oe. Inset (i–iii) shows the hysteresis loops measured at 300, 600 and 1,000 K showing coercivities of 150, 100 and 0 Oe, respectively



investigated in this work suggests that similar structure–magnetism relationship exists in this system also. More studies are required to elucidate the exact mechanism responsible for the destruction of ferromagnetism in our $\text{Ti}_{1-x}\text{Co}_x\text{O}_2$ for $x > 0.006$.

Figure 5 shows the variation of magnetization (normalized to the magnitude at 300 K) from 300 to 1,000 K for $\text{Ti}_{0.994}\text{Co}_{0.006}\text{O}_2$ sample under a constant applied field $H = 8,000$ Oe. The magnetization decreased with temperature and shows a change of slope near 675 K. Hysteresis loops collected at 300, 600 and 1,000 K, presented in the insets (i–iii) of Fig. 5, show clear coercivities which decrease with increasing temperature towards 675 K. This clearly indicate that 675 K is the blocking temperature of $\text{Ti}_{0.994}\text{Co}_{0.006}\text{O}_2$ above which it transforms from ferromagnetic phase with open hysteresis loops to superparamagnetic phase with zero coercivity. If the particles size is sufficiently small, above T_B thermal fluctuations dominate and particle can spontaneously switch magnetization. Such a system of superparamagnetic particle does not show hysteresis above T_B ; hence coercivity and remanant magnetization are zero although exhibiting the saturation magnetization as observed in Fig. 5(iii) [22, 23].

4 Conclusions

In conclusion, we report the development of room-temperature FM in chemically synthesized powder $\text{Ti}_{1-x}\text{Co}_x\text{O}_2$ samples with less than 0.6% Co. These samples exhibit hysteresis behavior with $\leq 0.2 \mu_B/\text{Co}$ magnetic moment. The $\text{Ti}_{0.994}\text{Co}_{0.006}\text{O}_2$ samples show a ferromagnetism upto the blocking temperature of 675 K and superparamagnetic behavior with further

increase in temperature. Co ion doping instigate the anatase to rutile phase transformation at relatively lower temperatures and systematically changes the structural and optical properties of TiO_2 .

Acknowledgements This research was supported in part by grants from, NSF-Idaho-EPSCoR program (EPS-0447689), Research Corporation, NSF-CAREER program (DMR-0449639) and the DoE-EPSCoR program (DE-FG02-04ER46142) at Boise State University. We are thankful to Jason Hays from Boise State University for helpful discussions and careful proof reading of the manuscript.

References

1. Y. Matsumoto, M. Murakami, T. Shono, T. Hasegawa, T. Fukumura, M. Kawasaki, P. Ahmet, T. Chikyow, S. Koshihara, H. Koinuma, *Science* **291**, 854 (2001)
2. S.R. Shinde, S.B. Ogale, S.D. Sarma, J.R. Simpson, H.D. Drew, S.E. Lofland, C. Lanci, J.P. Buban, N.D. Browning, V.N. Kulkarni, J. Higgins, R.P. Sharma, R.L. Greene, T. Venkatesan, *Phys. Rev. B* **67**, 115211 (2003)
3. J.D. Bryan, S.M. Heald, S.A. Chambers, D.R. Gamelin, *J. Am. Chem. Soc.* **126**, 11640 (2004)
4. H. Toyosaki, T. Fukumura, Y. Yamada, K. Nakjima, T. Chikyow, T. Hasegawa, H. Koinuma, M. Kawasaki, *Nat. Mater.* **3**, 221 (2004)
5. J.S. Higgins, S.R. Shinde, S.B. Ogale, T. Venkatesan, R.L. Green, *Phys. Rev. B* **69**, 073201 (2004)
6. W.K. Park, R.J. Ortega-Hertogs, J.S. Moodera, A. Punnoose, M.S. Seehra, *J. Appl. Phys.* **91**, 8093 (2002)
7. V. Shuthanandan, S. Thevuthasan, S.M. Heald, T. Droublay, M.H. Engelhard, T.C. Kasper, D.E. McCready, L. Saraf, S.A. Chambers, B.S. Mun, N.M. Hamdan, P. Nachimuthu, B. Taylor, R.P. Sears, B. Sinkovic, *Appl. Phys. Lett.* **84**, 4466 (2004)
8. J.Y. Kim, J.H. Park, B.G. Park, H.J. Noh, S.J. Oh, J.S. Yang, D.H. Kim, S.D. Bu, T.W. Noh, H.J. Lin, H.H. Heish, C.T. Chen, *Phys. Rev. Lett.* **90**, 017401 (2003)
9. K.A. Griffin, A.B. Pakamov, C.M. Wang, S.M. Heald, K.M. Krishnan, *Phys. Rev. Lett.* **94**, 157204 (2005)

10. M. Osada, Y. Ebina, K. Fukuda, K. Ono, K. Takada, K. Yamaura, E. Takayama-Muromachi, T. Sasaki, *Phys. Rev. B* **73**, 153301 (2006)
11. K.A. Griffin, M. Varela, S.J. Pennycook, A.B. Pachomov, K.M. Krsihnan, *J. Appl. Phys.* **99**, 08M114 (2006)
12. R.A. Spurr, H. Myers, *Anal. Chem.* **29**, 760 (1957)
13. R.D. Shannon, C.T. Prewitt, *Acta Crystallogr., Sect. B: Struct. Crystallogr. Cryst. Chem.* **25**, 925 (1969)
14. G. Kortum, *Reflectance Spectroscopy* (Springer-Verlag, New York, 1969)
15. D.A. Schwartz, N.S. Norberg, Q.P. Nguyen, J.M. Parker, D.R. Gamelan, *J. Am. Chem. Soc.* **125**, 13205 (2003)
16. N.H. Hong, W. Prellier, J. Sakai, A. Ruyter, *J. Appl. Phys.* **95**, 7378 (2004)
17. B.S. Jeong, Y.W. Heo, D.P. Norton, J.G. Kelly, R. Rairigh, A.F. Hebard, J.D. Budai, Y.D. Park, *Appl. Phys. Lett.* **84**, 2608 (2004)
18. S.A. Chambers, S. Thevuthasan, R.F.C. Farrow, R.F. Marks, J.U. Thiele, L. Folks, M.G. Samant, A.J. Kellock, N. Ruzycski, D.L. Ederer, U. Diebold, *Appl. Phys. Lett.* **79**, 3467 (2001)
19. J. Hays, A. Punnoose, R. Baldner, M.H. Engelhard, J. Peloquin, K.M. Reddy, *Phys. Rev. B* **72**, 075203 (2005)
20. J.M.D. Coey, A.P. Douvalis, C.B. Fitzgerald, M. Venkatesan, *Appl. Phys. Lett.* **84**, 1332 (2004)
21. J.M.D. Coey, M. Venkatesan, C.B. Fitzgerald, *Nat. Mater.* **4**, 173 (2005)
22. A. Punnoose, M. Seehra, N. Shah, T. Phanthavady, G.P. Huffman, *Phys. Rev. B* **69**, 054425 (2004)
23. M.S. Seehra, A. Punnoose, *Phys. Rev. B* **64**, 132410 (2001)